Scripta Materialia 213 (2022) 114619

Contents lists available at ScienceDirect

Scripta Materialia

journal homepage: www.journals.elsevier.com/scripta-materialia

# Engineering thermal hysteresis of ferromagnetic shape memory alloy sensory particles

W. Cho, D. Salas, N. Barta, I. Karaman *

*Department of Materials Science and Engineering, Texas A&M University, College Station, TX 77843, USA*

ARTICLE INFO

*Keywords:*
Ferromagnetic shape memory alloys
Shape memory particles
Martensitic transformation
Order-Disorder Transition
Hysteresis

ABSTRACT

Simultaneous magnetic and martensitic phase transitions in NiMn-based particles embedded in a metallic matrix could be stress-induced by crack propagation, making them candidates as sensory particles in structural health monitoring. For such applications, the particles should be small to maintain matrix properties, but large enough to martensitically transform at desired temperatures, requiring their transformation characteristics to be tailored. Here, the effects of heat treatments on the transformation characteristics of micron-sized $Ni_{45}Co_5Mn_{36.7}In_{13.3}$ particles are studied to demonstrate such tailorability. It is discovered that martensitic transformation temperatures are proportional to the annealing temperature below the order-disorder (ODO) transition and inversely proportional above it, and an opposite trend is observed for the transformation hysteresis. These findings are in agreement with the bulk behavior, however, a significantly larger hysteresis was found in the particles, which was correlated with crystallite size dependent phenomena, increasing the effective energy barrier to the phase-transition.

Ferromagnetic shape memory alloys (FSMAs) are known for their ability to undergo a reversible martensitic transformation (MT), leading to large changes in their magnetic properties. MT in these materials can be induced by temperature change and/or externally applied magnetic or stress fields [1–14]. It is widely known that NiMnX (X=In,Ga,Sn,Sb) Heusler alloys can display a noticeable change in magnetization upon MT [2,15]. Recently, few studies have explored the possibility of embedding FSMA particles into metal alloys to enable the detection of crack propagation throughout the material [16–18]. When a crack propagates through the material, it produces local stress fields which may be large enough to induce the MT in nearby FSMA particles. Since the MT is associated with a large change in the magnetic behavior of the particles, it is possible for the cracks to produce a magnetization change that can be measured externally. Then, FSMA particles embedded in metal alloys could be useful for structural health monitoring, complementing other techniques such as acoustic emission [19]. This magnetism-based sensing mechanism has been successfully demonstrated by embedding $Ni_{43}Co_7Mn_{39}Sn_{11}$ FSMA particles into pure aluminum [16,17].

FSMA particles should meet several requirements in order to enable or enhance their crack sensing capability, which are tied to their MT characteristics. Firstly, the unstressed particles should remain in austenite under normal operating conditions, so they may transform to martensite only by the effect of crack formation and growth. This requires martensite start temperature, $M_S$, to lie below the operating temperature range of the matrix alloy. Secondly, the critical stress required to induce the MT should be low, increasing the number of particles undergoing the MT at vicinity of cracks due to formation/expansion of crack stress-fields, and eventually enhancing sensitivity. Following the Clausius-Clapeyron relationship, $M_S$ should then not be far below the operating temperature range for keeping the critical transformation stress low. Thirdly, stressed particles in martensite should not transform back to austenite due to small temperature variations, meaning that austenite start temperature, $A_S$, should be above the operating temperature range, suggesting $A_S$ to be well-above room temperature (RT). Consequently, to widen the operating temperature range of the sensory particles, it is necessary to maximize the transformation thermal hysteresis, $\Delta T_{hys}=A_F-M_S$. Inconveniently, previous studies demonstrated that NiMnX alloys typically present MTs with thermal hysteresis of around 10–20 °C [20–22], which would generally be considered small for this particular sensing application. Fortunately, there are multiple strategies to engineer the MT temperatures and hysteresis in FSMAs, based on the control of composition [23–25] or thermal history [26–28].

* Corresponding author.
*E-mail address:* ikaraman@tamu.edu (I. Karaman).

https://doi.org/10.1016/j.scriptamat.2022.114619
Received 29 December 2021; Received in revised form 13 February 2022; Accepted 14 February 2022
Available online 23 February 2022

Thermal processing is often used to modify the crystal through B2-$L2_1$ order-disorder (ODO) transition occurring in the austenite. This strategy is viable when ODO critical temperature is relatively low, making it possible to modify the volume fraction of the ordered phase, $L2_1$, by performing heat treatments and quenching-in some of the B2 order present at the annealing temperature down to RT [26,29]. Since the degree of $L2_1$ order, $\eta_{L21}$, depends on temperature below ODO transition, different heat treatments can result in different degrees of B2/$L2_1$ order at RT. Due to dependence of ODO temperature on composition, this strategy is normally effective in NiMnIn [30] and NiMnGa [31], but not in NiMnSn and NiMnSb alloys [32].

Changes in $\eta_{L21}$ will modify the MT characteristics mostly by means of its notable impact on the magnetic properties of the material. The strength of the ferromagnetic interactions is stronger in ordered $L2_1$ phase than in B2 one, so the magnetic moment and Curie temperature of the austenite depend on the atomic ordering state [27]. The total MT entropy change, $\Delta s_{total}=s^{mar}-s^{aus}$, can be simplified as the sum of structural and magnetic contributions, $\Delta s_{total}=\Delta s_{strc.}+\Delta s_{mag}$, which are expected to present opposite signs for ferromagnetic (FM) austenite to paramagnetic (PM) martensite transition [33,34]. As a result, a certain heat treatment that increases $\eta_{L21}$ will increase the magnetization of the austenite in a NiCoMnIn alloy within MT range, increasing $\Delta s_{mag}$ and decreasing $\Delta s_{total}$ [29]. Such changes in the thermodynamic balance between austenite and martensite affect the MT temperatures and $\Delta T_{hys}$, as undercooling required for inducing the MT depends on driving force and total entropy change, $\Delta g = \Delta s_{total}\bullet\Delta T_{undercooling}\approx 1/2\bullet\Delta s_{total}\bullet\Delta T_{hys}$.

No systematic investigation on the effects of thermal processing, however, has been performed on FSMA particles, with a high surface-to-volume ratio, which is known to affect the MT characteristics [35–37]. Therefore, it is important to investigate: (1) how one can tailor the transformation characteristics of FSMA particles to optimize the sensing capabilities for structural health monitoring; (2) if and how the behavior of micron-sized particles differ from the bulk materials behavior; and (3) whether or not one can process FSMAs to exhibit wider transformation hysteresis while maintaining a high sensitivity to crack propagation.

In the present work, we have systematically investigated the

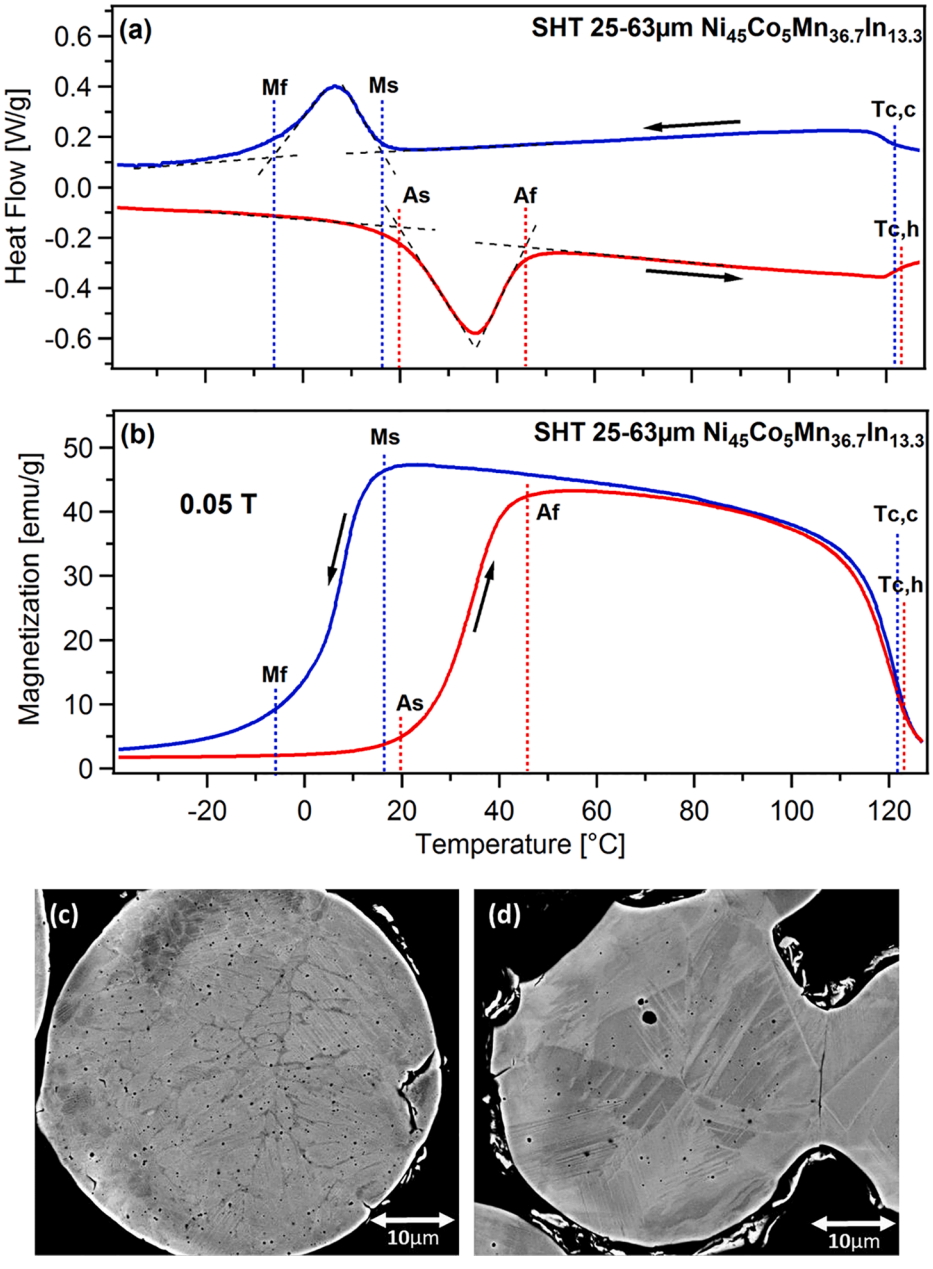


**Fig. 1.** (a) Calorimetric response of $Ni_{45}Co_5Mn_{36.7}In_{13.3}$ FSMA particles and the determination of transformation temperatures ($M_S$, $M_F$, $A_S$, $A_F$) and Curie temperature ($T_C$) using DSC, and (b) thermo-magnetic response obtained using SQUID confirming these temperatures. Backscattered electron images of 25–63 μm sized $NiMnCoIn_{13.3}$ particles in (c) as-gas-atomized and (d) solution heat treated (at 900 °C for 24 h) conditions, indicating the particle is chemically homogenized and consists of mixture of austenite and martensite phases.

dependence of magnetic and MT characteristics of micron-sized $Ni_{45}Co_5Mn_{36.7}In_{13.3}$ particles as a function of thermal processing temperature. The reason for the selection of this alloy is that its MT can produce a magnetization change higher than 100 emu/g under 1 T magnetic field, and its characteristic temperatures are tunable by controlling $\eta_{L21}$ via thermal processing [26,27,38], and the transformation temperatures of this particular composition is near RT. Therefore, this alloy allows us to investigate the dependence of $\Delta T_{hys}$ on thermal processing in FSMA particles and compare with the ones in the bulk samples.

Micron-sized particles with a nominal composition of $Ni_{45}Co_5Mn_{36.7}In_{13.3}$ at.% (denoted as $NiMnCoIn_{13.3}$) were fabricated using inert gas-atomization and sieved to sizes between 25 and 63 μm. To obtain samples with different heat-treatment (HT) conditions, the particles were sealed in separate quartz tubes under ultra-high purity argon. Specimens were initially solution heat treated (SHT) at 900 °C for 24 h for homogenization, and then water quenched (WQ) to RT without breaking the quartz tubes to minimize oxidation. Selected specimens were subsequently subjected to secondary HTs for 3 h at different temperatures (from 350 to 700 °C) to achieve different degrees of order.

A TA Instruments DSC Q2000 was utilized for measuring MT temperatures, $M_S$, $M_F$, $A_S$ and $A_F$, using the tangent line intersection method (Fig. 1(a)), the Curie temperature, $T_C$, total MT enthalpy and entropy changes, and for corroborating MT temperatures during thermal cycles, with a temperature rate of 10 °C/min, spanning both the ferromagnetic and martensitic transformations. For evaluating MT stability, both particle and bulk samples were prepared with the same thermal processing condition (400 °C, 3hr, WQ) and subjected to 10 thermal cycles spanning from -80 to 80 °C covering the entire MT range with a cooling/heating rate of 10 °C/min. The sample demonstrated a decrease in $\Delta T_{hys}$ from Cycle 1 to 10 of 5 and 7 °C, respectively. This particular thermal processing condition was selected in order to achieve $M_S$ around the room temperature. Thermomagnetic response was measured during temperature cycles under constant applied fields ranging from 0.05 to 5 T using a Quantum Design MPMS SQUID-VSM magnetometer.

The evolution of magnetization during isothermal holding experiments was used to investigate the isothermal MT behavior of the particle and bulk samples in 400 °C, 3 h, WQ condition. Each sample was first heated up above $A_F$, cooled down to the target temperature at 2 °C/min, and held isothermally for 40 min. Different isothermal stops were implemented during the same temperature cycle, with at least 20 °C between each stop. This cycle was repeated multiple times covering the entire forward MT temperature range. The isothermal MT rate $Z$, was then calculated as

$$\frac{\Delta m_{iso}}{\Delta m_{tr}} = -Zln(t) \quad (1)$$

where $\Delta m_{iso}$ is the accumulated magnetization change at a given time, $t$, after the temperature ramp was interrupted; $\Delta m_{tr}$ is the total magnetization difference between austenite and martensite; and $\Delta m_{iso}/\Delta m_{tr}$ is an approximation for the isothermal change in martensite volume fraction, $\Delta F_{iso}$ [39–41].

Scanning electron microscopy (SEM) images, captured using a FEI Quanta 600 SEM, were used to investigate the microstructure changes Fig. 1.(c) and (d) present Back Scattered Electron (BSE) images of the as-atomized and homogenized particles. Clearly, SHT at 900 °C for 24 h eliminated the dendritic structures, which are known to restrict martensite growth.

Composition analysis of the homogenized particle and bulk samples were measured using wavelength dispersive X-Ray spectroscopy (WDS) in a Cameca SXFive EPM. The average measured composition of SHT particle and bulk samples are $Ni_{44.81\pm0.19}Co_{4.95\pm0.05}Mn_{36.66\pm0.20}In_{13.58\pm0.04}$ and $Ni_{44.94\pm0.19}Co_{4.98\pm0.06}Mn_{36.33\pm0.24}In_{13.76\pm0.09}$, respectively. Both materials were quite homogeneous as standard deviation of chemical analysis was low and there was no composition gradient.

*In-situ* high-energy synchrotron XRD experiments were conducted at the Advanced Photon Source, Argonne National Laboratory on $NiCoMnIn_{13.3}$ bulk material. SHT samples were heated to different temperatures below the ODO transition temperature, and then held isothermally. During this process, polar diffraction patterns were recorded in regular time-intervals. The relative volume fraction of $L2_1$ phase at different temperatures was calculated by comparing the square root of the total intensity of $(111)_{L21}$ diffraction spots at annealing temperature and the initial intensity in SHT state for estimating the temperature dependence of the $\eta_{L21}$.

Fig. 2 presents the dependence of MT temperatures, $\Delta T_{hys}$, and $T_C$ on thermal processing conditions for $NiMnCoIn_{13.3}$, comparing the results between particles and bulk samples, where grain sizes are of the order of millimeter Fig. 2.(a) shows that the transformation temperatures of the particles increase non-linearly with increasing annealing temperature from 350 to 550 °C and then decrease for annealing temperatures between 550 and 900 °C. The same behavior was observed for the bulk samples (Fig. 2(b)). $\Delta T_{hys}$ of both particle and bulk samples presents the opposite tendency with annealing temperature and a minimum occurs at a temperature close to 550 °C (Fig. 2(c)). Furthermore, one can observe in Fig. 2(d) that $T_C$ also presents a minimum with HT temperature.

The distribution of Mn/In atoms in ordered $L2_1$ structure results in stronger ferromagnetic interactions than in B2 phase. Therefore, we expect a positive correlation between $T_C$ and $\eta_{L21}$ [27]. To corroborate this relationship, we had previously determined the temperature-dependence of volume fraction of $L2_1$ phase using *in-situ* synchrotron measurements in bulk $NiMnCoIn_{13.3}$ [28], which is also included in Fig. 2(d). The good correlation between the change of $\eta_{L21}$ and $T_C$ as a function of the HT suggests that the change of the MT properties in Fig. 2 should be dominated by the variation of $\eta_{L21}$. A similar correlation can be established among the $\eta_{L21}$, MT temperatures and $\Delta T_{hys}$, resulting in observed maxima and minima in Fig. 2(a)–(c).

As in Ni-Mn-Ga [42] or Ni-Fe-Ga [43] alloys, these non-monotonic behaviors originate from the non-monotonic dependence of the after-quench $\eta_{L21}$ on annealing temperature since the formation of $L2_1$ phase presents a different "pathway" below and above ODO temperature. Below the ODO temperature, after-quench $\eta_{L21}$ will be similar to the pre-quench thermal equilibrium state since the ordering kinetics are too slow to produce a significant change during the quenching below 500 °C [44]. Note that ODO transition is a second order transformation, and the order parameter is expected to decrease with increasing temperature [25,45]. Therefore, $\eta_{L21}$ for the samples annealed below ODO transition should decrease on increasing annealing temperature. By contrast, $L2_1$ phase is not stable above the ODO transition, and thus after-quench $\eta_{L21}$ should be produced during the fast cooling. In this case, after-quench $\eta_{L21}$ increases on increasing annealing temperature above the ODO transition due to a larger vacancy concentration in the material. Vacancies promote atomic diffusion, so increasing its concentration results in faster kinetics of the B2→$L2_1$ ordering [42,43]. Altogether, after-quench $\eta_{L21}$ is expected to be at a minimum for HT temperatures close to ODO transition temperature, determined as 627 °C for bulk $NiMnCoIn_{13.3}$ [26].

Another important point in Fig. 2 is that $\Delta T_{hys}$ of the particles is significantly larger than that for the bulk samples. This arises from the different crystallite size of particles (25–63 μm) and bulk samples (up to few millimeters). Firstly, a different crystallite size imply that they will contain different defect populations, affecting the likelihood of these defects acting as high energy sites for the nucleation of martensite. On decreasing crystallite size, the probability to find nucleation sites permitting the formation of stable martensite nuclei is reduced, so the MT has a low nucleation site potency. This scenario can be represented as an effective increase of the energy barriers opposing the transformation, which will require an increase of the free energy to be overcome. As a result, the particles will require a larger undercooling to undergo MT, decreasing $M_S$ and increasing $\Delta T_{hys}$ [46].

Secondly, a larger $\Delta T_{hys}$ may be a consequence of enhanced frictional dissipated energy, produced via different irreversible processes during

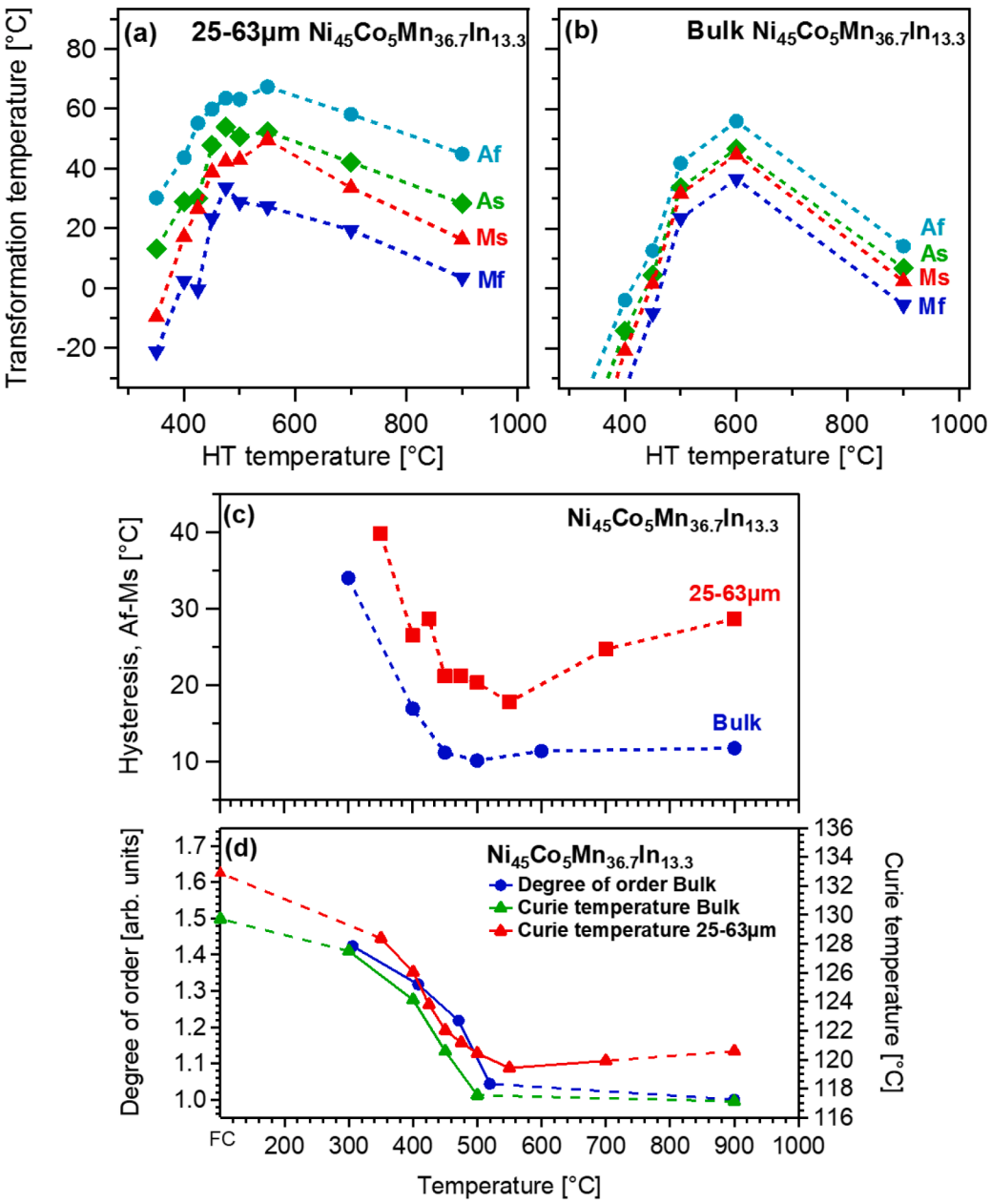


**Fig. 2.** Effect of annealing temperature on the MT temperatures of (a) 25–63 μm sized $NiMnCoIn_{13.3}$ particles and of (b) bulk $NiMnCoIn_{13.3}$, and on (c) their transformation hysteresis and (d) the degree of order and Curie temperature. All HTs were performed for 3 h.

the MT. Some examples are (i) the interaction of the MT interface with point defects, dislocations, interface boundaries, like B2-$L2_1$ order domain and grain boundaries [47]; (ii) the creation of dislocations to accommodate transformation shear and volume change; or (iii) the dissipation of energy as heat or acoustic emission. According to [48], one can relate the frictional contribution to the MT free energy difference, $\Delta g_{fr}$, with MT temperatures and total entropy difference:

$$\Delta T_{hys} \cong 2 \cdot \Delta g_{fr} / \Delta s_{total} \quad (2)$$

Fig. 3(a) and (b) presents the experimentally measured hysteresis and $\Delta s_{total}$ as a function of the ferromagnetic temperature range, $T_C$-$M_S$. Interestingly, $\Delta s_{total}$ for particle and bulk samples present similar magnitude and dependence on $T_C$-$M_S$ difference. This evidence indicates that MT in the particles has a similar balance between magnetic and non-magnetic contributions to $\Delta s_{total}$ as in the bulk samples, and thus changes in $\eta_{L21}$ via thermal processing have a similar impact on MT thermodynamics. Following, one can use Eq. (2) for obtaining a rough estimation of the frictional free energy, which is shown in Fig. 3(c). Given that there is not a significant difference in $\Delta s_{total}$, frictional work during the MT in particle samples can be up to 3 times larger than the one for the bulk samples. Furthermore, after thermocycling particle and bulk samples for 10 cycles, both annealed at 400 °C for 3 h, $M_S$ increased about 9 and 7 °C and $\Delta T_{hys}$ decreased about 7 and 5 °C, respectively; and transformation range $M_S$-$M_F$ was on average 20 and 15 °C for the same cases. These data suggest a more complicated martensite accommodation in the particles, requiring a higher density of martensite twin boundaries and defect creation.

Lastly, the forward MT of $NiMnCoIn_{13.3}$ has been shown to exhibit an isothermal behavior [39]. Therefore, $\Delta T_{hys}$ should be rate dependent. To understand the possible size effects on the isothermal behavior, the first temperature derivative of the magnetization during an uninterrupted cycle and the isothermal magnetization change rate during isothermal holding experiments ($Z$ parameter, Eq. (1)) was compared for two similar particle and bulk samples (see Fig. 4 and its caption for details).

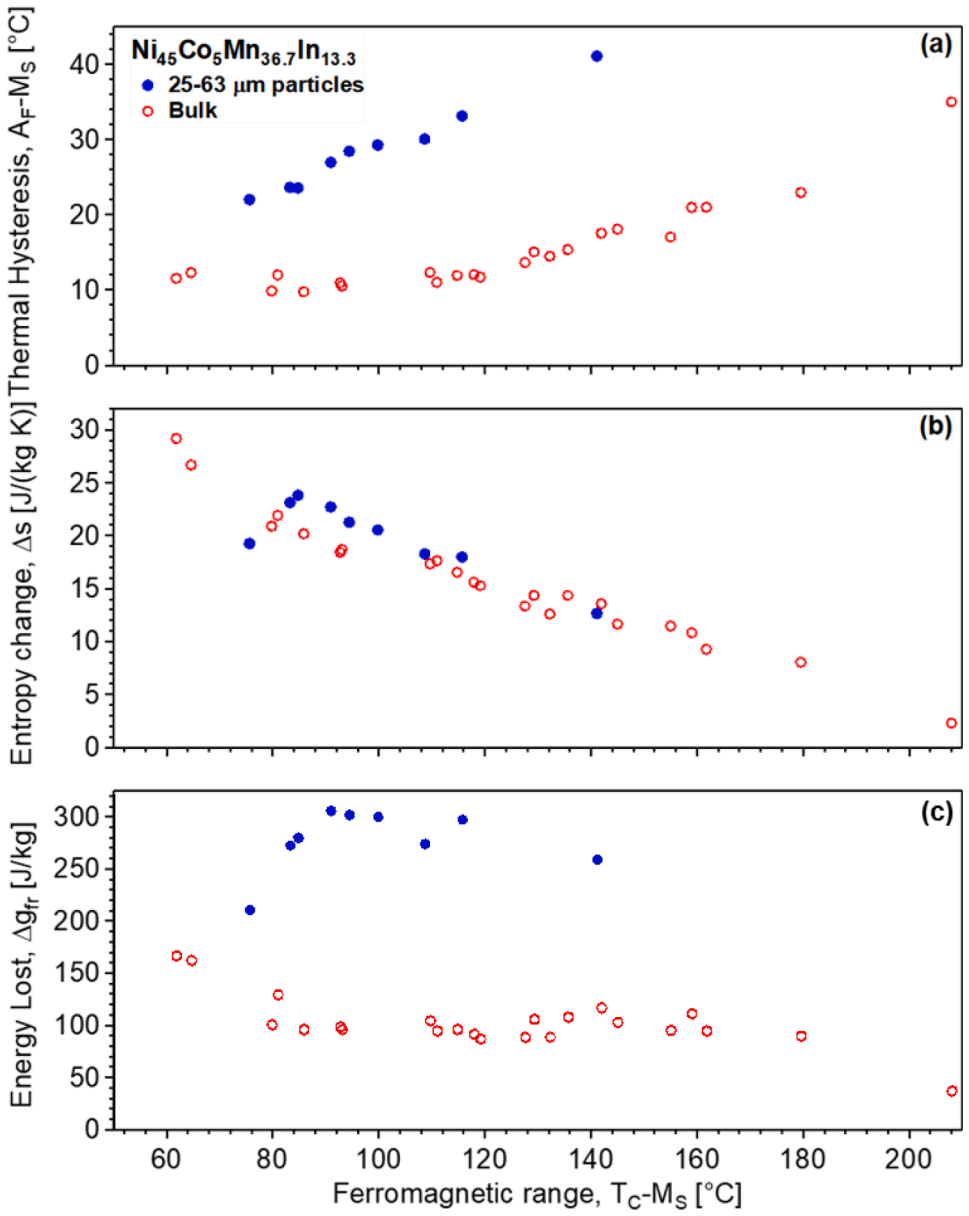


**Fig. 3.** Measured or calculated thermodynamic variables in the temperature range of ferromagnetic behavior in 25–63 μm sized $NiMnCoIn_{13.3}$ particles and bulk samples: (a) thermal hysteresis (b) entropy change and (c) frictional work (irreversible free energy).

Interestingly, isothermal accumulation of martensite of the micron-sized particles was significantly lower than that of the bulk samples. This result suggests that formation of martensite by means of thermally activated processes is minor in the particles, and thus their MT proceeds mostly athermally. An increase of the effective elastic energy barriers on reducing particle size should reduce the likelihood of thermal activated events, decreasing $Z$. Still, $\Delta T_{hys}$ dependence on heating/cooling rate for the particles and bulk samples is on the order of few degrees, notably lower than the observed three-fold difference between the particles and bulk samples. Therefore, the lack of isothermal martensite in the particles should be a minor contribution to the increase in $\Delta T_{hys}$.

Altogether, we suggest that the increased $\Delta T_{hys}$ in the $NiCoMnIn_{13.3}$ particles is mainly a product of a reduced nucleation site potency and an increased energy dissipation during formation and accommodation of martensite variants/twins. Both phenomena result in enhanced effective elastic energy barriers. These mechanisms may also result in more defect creation and lack of isothermal martensite, which should have a secondary contribution towards extending $\Delta T_{hys}$.

In summary, the effects of annealing heat treatments on the MT characteristics of micron-sized $Ni_{45}Co_5Mn_{36.7}In_{13.3}$ particles depend strongly on annealing temperature, resulting in a non-monotonic behavior for MT temperatures and $\Delta T_{hys}$, which respectively present a maximum or a minimum close to ODO transition temperature. These are, in general, the same trends observed previously on bulk samples, which are correlated with variations of after-quench volume fraction of ordered $L2_1$ phase since it affects the magnetism of austenite phase and its stability. For the same annealing conditions, a larger thermal hysteresis is found in particles than in bulks. It is suggested that the smaller crystalline size of the particles is associated with thermodynamic constraints for martensite variants, causing a change in MT frictional work and isothermal transformation behavior in the particles. Overall, the size reduction in $Ni_{45}Co_5Mn_{36.7}In_{13.3}$ to a micron level has a significant effect on MT temperatures and $\Delta T_{hys}$, due to the increased frictional work. The particle size and degree of order, controlled via annealing temperatures, provide a control knob to tailor $\Delta T_{hys}$ of this potential sensory particle to be utilized in structural health monitoring.

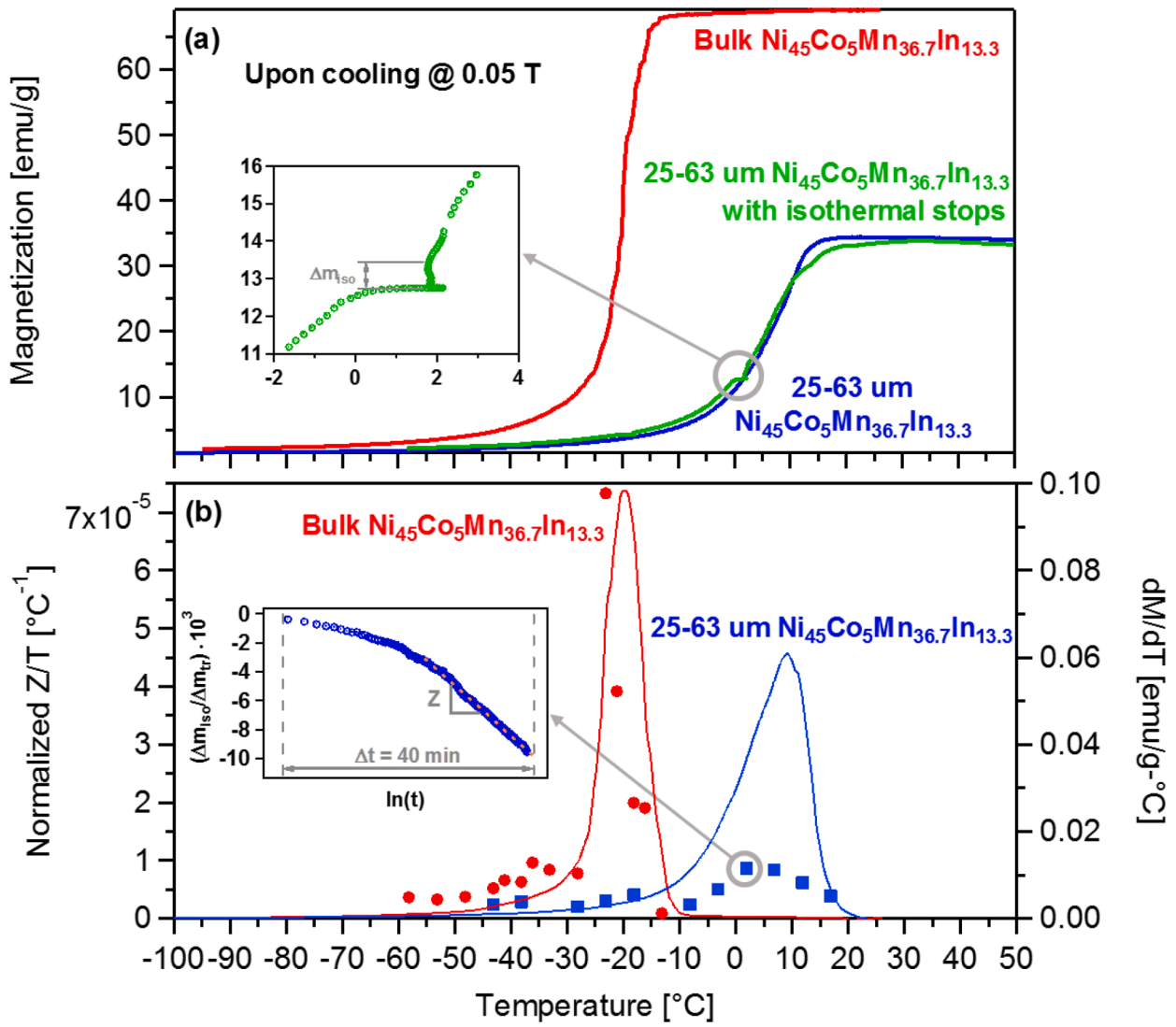


**Fig. 4.** Isothermal magnetization change during martensitic transformation and thermomagnetic behavior of $NiMnCoIn_{13.3}$ heat treated at 400 °C for 3 h. (a) shows the magnetization change over temperature upon cooling under 0.05 T for both the bulk sample (red) and the 25–63 μm particles (blue) with another curve with an example of an isothermal stop at 2 °C (green and inset, the isothermal hold is for 2400 s) for the particles. (b) compares the temperature derivative of the magnetization (the right y-axis), obtained from (a), for the bulk sample (red line) and the particles (blue line) and isothermal effects at each designated temperature stops (the left y-axis) for the bulk sample (red dots) and the particles (blue dots). Z, isothermal magnetization change rate during isothermal holding, was normalized by dividing it by the hold temperature yielding the relative magnitude of the isothermal effects. The inset in (b) presents an example of isothermal accumulation of martensite for the particles at 2 °C (indicated by gray circle), where linear interpolation method was used with the magnetization change ratio, $\Delta m_{iso}/\Delta m_{tr}$, with logarithmic time, ln(t), during 40 min of isothermal hold, Δt, to calculate the Z parameter using Eq. (1).

## Declaration of Competing Interest

The authors declare that they have no known competing financial interests or personal relationships that could have appeared to influence the work reported in this paper.

## Acknowledgments

This work was supported by The U.S. National Science Foundation, Division of Materials Research, Grant No. 1905325.

## References

[1] K. Ullakko, J. Huang, C. Kantner, R. O'handley, V.J.A.P.L. Kokorin, Large magnetic-field-induced strains in $Ni_2MnGa$ single crystals, Appl. Phys. Lett. 69 (1996) 1966–1968.
[2] A. Sozinov, A.A. Likhachev, N. Lanska, K. Ullakko, Giant magnetic-field-induced strain in NiMnGa seven-layered martensitic phase, Appl. Phys. Lett. 80 (2002) 1746–1748.
[3] R. Kainuma, Y. Imano, W. Ito, H. Morito, Y. Sutou, K. Oikawa, A. Fujita, K. Ishida, S. Okamoto, O. Kitakami, Metamagnetic shape memory effect in a Heusler-type $Ni_{43}Co_7Mn_{39}Sn_{11}$ polycrystalline alloy, Appl. Phys. Lett. 88 (2006), 192513.
[4] H.E. Karaca, I. Karaman, B. Basaran, Y.J. Chumlyakov, H.J. Maier, Magnetic field and stress induced martensite reorientation in NiMnGa ferromagnetic shape memory alloy single crystals, Acta Mater. 54 (2006) 233–245.
[5] I. Karaman, B. Basaran, H.E. Karaca, A.I. Karsilayan, Y.I. Chumlyakov, Energy harvesting using martensite variant reorientation mechanism in a NiMnGa magnetic shape memory alloy, Appl. Phys. Lett. 90 (2007), 172505.
[6] B. Kiefer, H.E. Karaca, D.C. Lagoudas, I. Karaman, Characterization and modeling of the magnetic field-induced strain and work output in Ni2MnGa magnetic shape memory alloys, J. Magn. Magn. Mater. 312 (2007) 164–175.
[7] R. Kainuma, K. Oikawa, W. Ito, Y. Sutou, T. Kanomata, K. Ishida, Metamagnetic shape memory effect in NiMn-based Heusler-type alloys, J. Mater. Chem. 18 (2008) 1837–1842.
[8] H. Karaca, I. Karaman, A. Brewer, B. Basaran, Y. Chumlyakov, H. Maier, Shape memory and pseudoelasticity response of NiMnCoIn magnetic shape memory alloy single crystals, Scr. Mater. 58 (2008) 815–818.
[9] H.E. Karaca, I. Karaman, B. Basaran, Y. Ren, Y.I. Chumlyakov, H.J. Maier, Magnetic Field-Induced Phase Transformation in NiMnCoIn Magnetic Shape-Memory Alloys–A New Actuation Mechanism with Large Work Output, Adv. Funct. Mater. 19 (2009) 983–998.

[10] R. Kainuma, K. Ito, W. Ito, R. Umetsu, T. Kanomata, K. Ishida, NiMn-based metamagnetic shape memory alloys, Mater. Sci. Forum 635 (2010) 23–31.

[11] J. Monroe, I. Karaman, B. Basaran, W. Ito, R. Umetsu, R. Kainuma, K. Koyama, Y. Chumlyakov, Direct measurement of large reversible magnetic-field-induced strain in Ni–Co–Mn–In metamagnetic shape memory alloys, Acta Mater. 60 (2012) 6883–6891.

[12] N.M. Bruno, C. Yegin, I. Karaman, J.H. Chen, J.H. Ross, J. Liu, J.G. Li, The effect of heat treatments on $Ni_{43}Mn_{42}Co_4Sn_{11}$ meta-magnetic shape memory alloys for magnetic refrigeration, Acta Mater. 74 (2014) 66–84.

[13] B. Emre, N.M. Bruno, S.Y. Emre, I. Karaman, Effect of niobium addition on the martensitic transformation and magnetocaloric effect in low hysteresis NiCoMnSn magnetic shape memory alloys, Appl. Phys. Lett. 105 (2014), 231910.

[14] APA: Bruno, N. M. (2015). The magnetocaloric and elastocaloric effects in magnetic shape memory alloys. Texas A&M University. https://oaktrust.library.tamu.edu/handle/1969.1/155374.

[15] R. Kainuma, Y. Imano, W. Ito, Y. Sutou, H. Morito, S. Okamoto, O. Kitakami, K. Oikawa, A. Fujita, T. Kanomata, K. Ishida, The magnetocaloric and elastocaloric effects in magnetic shape memory alloys, Nature 439 (2006) 957–960.

[16] N. Barta, I. Karaman, Magnetic-field-induced shape recovery by reverse phase transformation, Mater. Sci. Eng. A 751 (2019) 201–213.

[17] N.E. Barta, C. Fincher, A.M. Bolon, V. Attari, W. Higgins, R. Arroyave, M. Radovic, G.M. Pharr, I. Karaman, Embedded magnetic shape memory sensory particles in lightweight composites for crack detection, Mater. Sci. Eng. A 805 (2021), 140549.

[18] N.M. Samy, M.K. Bolgár, N. Barta, L. Daróczi, L.Z. Tóth, Y.I. Chumlyakov, I. Karaman, D.L. Beke, Fabrication and characterization of aluminum - magnetic shape memory alloy composites, J. Alloy. Compd. 778 (2019) 669–680.

[19] W. Leser, J. Newman, J. Hochhalter, V. Gupta, F. Yuan, Thermal, acoustic and magnetic noises emitted during martensitic transformation in single crystalline $Ni_{45}Co_5Mn_{36.6}In_{13.4}$ meta-magnetic shape memory alloy, Fatigue Fract. Eng. Mater. struct. 39 (2016) 686–695.

[20] W. Ito, Y. Imano, R. Kainuma, Y. Sutou, K. Oikawa, K. Ishida, Embedded Ni–Ti particles for the detection of fatigue crack growth in AA7050, Metall. Mater. Trans. A 38 (2007) 759–766.

[21] C. Jiang, Y. Muhammad, L. Deng, W. Wu, H. Xu, Martensitic and Magnetic Transformation Behaviors in Heusler-Type NiMnIn and NiCoMnIn Metamagnetic Shape Memory Alloys, Acta Mater. 52 (2004) 2779–2785.

[22] S.K. Wu, S.T. Yang, Composition dependence on the martensitic structures of the Mn-rich NiMnGa alloys, Mater. Lett. 57 (2003) 4291–4296.

[23] V. Chernenko, Effect of composition on transformation temperatures of Ni–Mn–Ga shape memory alloys, Scr. Mater. 40 (1999) 523–527.

[24] X. Moya, L. Mañosa, A. Planes, T. Krenke, M. Acet, E.F. Wassermann, Compositional instability of β-phase in Ni-Mn-Ga alloys, Mater. Sci. Eng. A 438 (2006) 911–915.

[25] V. Recarte, J. Pérez-Landazábal, V. Sánchez-Alarcos, J. Rodríguez-Velamazán, Martensitic transition and magnetic properties in Ni–Mn–X alloys, Acta Mater. 60 (2012) 1937–1945.

[26] N.M. Bruno, D. Salas, S. Wang, I.V. Roshchin, R. Santaniarta, R. Arroyave, T. Duong, Y.I. Chumlyakov, I. Karaman, Dependence of the martensitic transformation and magnetic transition on the atomic order in Ni–Mn–In metamagnetic shape memory alloys, Acta Mater. 142 (2018) 95–106.

[27] D. Salas, O. Eliseeva, Y. Wang, T. Duong, Y. Chumlyakov, Y. Ren, R. Arroyave, I. Karaman, On the microstructural origins of martensitic transformation arrest in a NiCoMnIn magnetic shape memory alloy, Acta Mater. 166 (2019) 630–637.

[[28]] D. Salas, Y. Wang, T.C. Duong, V. Attari, Y. Ren, Y. Chumlyakov, R. Arroyave, I. Karaman, Effects of composition and crystallographic ordering on the ferromagnetic transition in NiCoMnIn magnetic shape memory alloys, Acta Mater. 206 (2021) 116616.

[29] W. Ito, M. Nagasako, R. Umetsu, R. Kainuma, T. Kanomata, K. Ishida, Competing Interactions between Mesoscale Length-Scales, Order-Disorder, and Martensitic Transformation in Ferromagnetic Shape Memory Alloys, Appl. Phys. Lett. 93 (2008), 232503.

[30] S. Kustov, M.L. Corró, J. Pons, E. Cesari, Atomic ordering and magnetic properties in the $Ni_{45}Co_5Mn_{36.7}In_{13.3}$ metamagnetic shape memory alloy, Appl. Phys. Lett. 94 (2009), 191901.

[31] V. Sánchez-Alarcos, V. Recarte, J.I. Pérez-Landazábal, G.J. Cuello, Entropy change and effect of magnetic field on martensitic transformation in a metamagnetic Ni–Co–Mn–In shape memory alloy, Acta Mater. 55 (2007) 3883–3889.

[32] V. Sánchez-Alarcos, J.I. Pérez-Landazábal, V. Recarte, I. Lucia, J. Vélez, J. A. Rodríguez-Velamazán, Correlation between atomic order and the characteristics of the structural and magnetic transformations in Ni–Mn–Ga shape memory alloys, Acta Mater. 61 (2013) 4676–4682.

[33] R.Y. Umetsu, W. Ito, K. Ito, K. Koyama, A. Fujita, K. Oikawa, T. Kanomata, R. Kainuma, K. Ishida, Effect of high-temperature quenching on the magnetostructural transformations and the longrange atomic order of Ni–Mn–Sn and Ni–Mn–Sb metamagnetic shape memory alloys, Scr. Mater. 60 (2009) 25–28.

[34] C. Seguí, E. Cesari, Anomaly in entropy change between parent and martensite phases in the Ni50Mn34In16 Heusler alloy, Entropy 16 (2014) 5560–5574.

[35] M. Chmielus, K. Rolfs, R. Wimpory, W. Reimers, P. Müllner, R. Schneider, Contributions to the transformation entropy change and influencing factors in metamagnetic NiCo-Mn-Ga shape memory alloys, Acta Mater. 58 (2010) 3952–3962.

[36] N. Jetta, N. Ozdemir, S. Rios, D. Bufford, I. Karaman, X. Zhang, Effects of surface roughness and training on the twinning stress of Ni–Mn–Ga single crystals, Thin Solid Films 520 (2012) 3433–3439.

[37] N. Ozdemir, I. Karaman, N.A. Mara, Y.I. Chumlyakov, H.E. Karaca, Size effects in the superelastic response of $Ni_{54}Fe_{19}Ga_{27}$ shape memory alloy pillars with a two stage martensitic transformation, Acta Mater. 60 (2012) 5670–5685.

[38] W. Ito, R.Y. Umetsu, R. Kainuma, T. Kakeshita, K. Ishida, Heat-induced and isothermal martensitic transformations from kinetically arrested parent phase in NiCoMnIn metamagnetic shape memory alloy, Scr. Mater. 63 (2010) 73–76.

[39] S. Kustov, I. Golovin, M.L. Corró, E. Cesari, Isothermal martensitic transformation in metamagnetic shape memory alloys, J. Appl. Phys. 107 (2010), 053525.

[40] J.I. Pérez-Landazábal, V. Recarte, V. Sánchez-Alarcos, S. Kustov, D. Salas, E. Cesari, Intermetallics 28 (2012) 144–148.

[41] J.I. Pérez-Landazábal, V. Recarte, J. Torrens-Serra, E. Cesari, Relaxation effects in magnetic-field-induced martensitic transformation of an Ni–Mn–In–Co alloy, Acta Mater. 71 (2014) 117–125.

[42] V. Sanchez-Alarcos, J.I. Perez-Landazabal, V. Recarte, J.A. Rodriguez-Velamazan, V.A. Chernenko, Effect of atomic order on the martensitic and magnetic transformations in Ni-Mn-Ga ferromagnetic shape memory alloys, J. Phys. Condens. Matter 22 (2010), 166001.

[43] R. Santamarta, E. Cesari, J. Font, J. Muntasell, J. Pons, J. Dutkiewicz, Effect of atomic order on the martensitic transformation of Ni–Fe–Ga alloys, Scr. Mater. 54 (2006) 1985–1989.

[44] Y. Wang, C.H. Huang, J.H. Gao, S. Yang, X.D. Ding, X.P. Song, X.B. Ren, Evidence for ferromagnetic strain glass in Ni-Co-Mn-Ga Heusler alloy system, Appl. Phys. Lett. 101 (2012).

[45] A. Planes, L. Manosa, E. Vives, J. Rodriguezcarvajal, M. Morin, G. Guenin, J. L. Macqueron, Neutron-Diffraction Study of Long-Range Atomic Order in Cu-Zn-Al Shape Memory Alloys, J. Phys. Condens. Matter 4 (1992) 553–559.

[46] Y. Zhang, C. Lago, I. Karaman, P.J. Shamberger, Nucleation site potency distributions in thermoelastic martensitic transformation $Ni_{43}Co_7Mn_{39}Sn_{11}$ particles, Phys. Rev. Mater. 5 (2021), 023401.

[47] A. Roitburd, Martensitic transformation as a typical phase transformation in solids. Solid State Physics, Elsevier, 1978, pp. 317–390.

[48] E.Y. Panchenko, Y.I. Chumlyakov, I. Kireeva, A. Ovsyannikov, H. Sehitoglu, I. Karaman, Y.J. Maier, Effect of disperse $Ti_3N_4$ particles on the martensitic transformations in titanium nickelide single crystals, Phys. Met. Metallogr. 106 (2008) 577.